Solvation Dynamics in Liquid Water. III. Energy Fluxes and Structural Changes

Rossend Rey[*][*]

Departament de Física, Universitat Politècnica de Catalunya, Campus Nord B4-B5, Barcelona 08034, Spain.

James T. Hynes[*][†]

Department of Chemistry and Biochemistry, University of Colorado, Boulder, CO 80309-0215 USA,
Ecole Normale Supérieure-PSL Research University,
Chemistry Department, Sorbonne Universités-UPMC University Paris 06,
CNRS UMR 8640 Pasteur, 24 rue Lhomond, 75005 Paris, FR

(Dated: January 16, 2017)

ABSTRACT: In previous installments it has been shown how a detailed analysis of energy fluxes induced by electronic excitation of a solute can provide a quantitative understanding of the dominant molecular energy flow channels characterizing solvation—and in particular, hydration— relaxation dynamics. Here this work and power approach is complemented with a detailed characterization of the changes induced by such energy fluxes. We first examine the water solvent's spatial and orientational distributions and the assorted energy fluxes in the various hydration shells of the solute to provide a molecular picture of the relaxation. The latter analysis is also used to address the issue of a possible "inverse snowball" effect, an ansatz concerning the time scales of the different hydration shells to reach equilibrium. We then establish a link between the instantaneous torque, exerted on the water solvent neighbors' principal rotational axes immediately after excitation and the final energy transferred into those librational motions, which are the dominant short-time energy receptor.

I. INTRODUCTION

In previous contributions (Refs. 1,2, hereafter denoted I and II respectively), we presented a novel perspective to address the time-dependent frequency shift that results from electronic excitation of a chromophore in solution, typically termed "solvation dynamics".[3–11] This approach involves the computation of the nonequilibrium energy fluxes induced by the initial electronic excitation of a solute, a methodology previously implemented for vibrational/rotational relaxation.[12–14] Its central merit is its ability to provide unambiguous quantitative information about the participation of each solvent molecule, information which can be further combined to discuss the participation of groups of molecules (hydration/solvation shells) or modes (vibration/rotation/translation). Its first application to solvation dynamics in I was to the classic idealized model system of an initially neutral monatomic solute in water which instantaneously acquires a positive/negative unit charge.[15–26] In II, the formalism was extended to the general case, for which both excited and ground electronic states of the solute are characterized by finite charge distributions.

I and II provided the first quantitative estimation of the participation of each water solvent molecular mode (vibrations, librations, i.e. hindered rotations, translations) and each ionic hydration shell. After the initial excitation, water molecule librations channel approximately three fourths of the substantial initially created Coulomb energy perturbation (*vide infra*), while translations account for the rest, with the water vibrations playing a negligible role. In addition, the rotational/librational energy flow proceeds in a non-symmetric fashion in the principal axes, with rotations around the axis parallel to the molecule's H-H axis accounting for most of the energy flow[1] (its share fluctuates in the environ of $\sim 75\%$ of the energy transferred, depending on ionic charge and hydration shell considered). Finally, the expected dominant role of first hydration shell molecules was explicitly established, with roughly two thirds of the total energy flowing directly into the molecules closest to the newly formed ion.
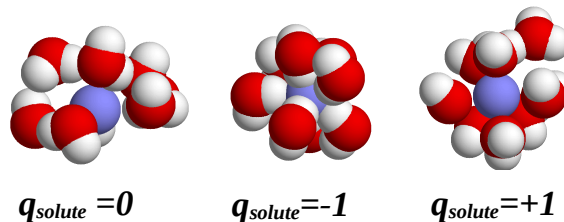

FIG. 1: Snapshots of the closest eight water molecules and the central solute (blue).

This short account reflects that the focus so far has been on identifying the main energy flow channels for relaxation. In this contribution, we shift the focus to the scrutiny of how the substantial energy fluxes that they entail—of up to ~ 10 kcal/mol per molecule, for the closest water molecules—translate into structural changes, which can be rather dramatic for the aqueous systems studied. Indeed, acquisition of a net charge by the solute will surely result in major reorientation and center of mass shifts for the water molecules in the solute's immediate vicinity and beyond, due to the well-known substantial hydration layer structural differences for ions and neutral solutes (see Fig. 1 for an illustration). Such changes will take place over extremely short periods of

time, during which a substantial amount of Coulomb energy is redistributed, of the order of 100 kcal/mol. For example, $\approx 70\%$ of the relaxation is over in a time of ~ 20 fs.[1] Not all solvent molecules will respond on the same time scale, since the forces and torques generated by the electronic transition will differ, and it is of interest to characterize these aspects on a molecular level.

In the present effort, we will first seek a molecular level mechanistic understanding of the substantial structural rearrangements that take place in the water solvent. The unfolding of the orientational and positional changes after electronic excitation can be monitored through inspection of the time dependence of the radial distribution function ($g(r)$) and similar functions that characterize orientational correlation, which provides a more visual perspective on the problem of solvation dynamics. We will find though that, informative as such analysis is, an energy flow analysis provides a more explicit description of the different molecular motions involved, i.e. the translational and librational water solvent motions and their dependence on the solute hydration shell. The first half of the present work will be devoted to these issues.

There is an interesting further related aspect—directly connected to the spatial and time sequence of the aqueous solvent relaxation—that we address at the end of the first half of this contribution, which we now motivate. The typical expectation is that those molecules subject to a lesser perturbation, and therefore further away from the solute, would equilibrate more readily. However, how the time scale for solvation relaxation depends on the distance from the solute is in fact a topic that has received much attention. Probably the important motivation here came from a well-known comment by Onsager, suggesting that the solvent electric polarization structure around an *electron* might proceed from outside in; in this "inverse snowball effect" (ISE), it is the less perturbed molecules that would adjust more rapidly. To the best of our knowledge the ISE has not been found computationally for *atomic/molecular* solutes in water, although there were some initial computational hints,[27,28] followed by a number of theoretical discussions arguing against the ISE in polar solvents, e.g. see Refs. 29,30. In fact, a computational study of relaxation in liquid tetrahydrofuran,[31] appears to have found the opposite, "snowball" effect (see reference 51 of Ref. 31), supporting a prediction made for systems dominated by translational relaxation.[29] The absence of an ISE was found for simulated acetonitrile[32] and for Stockmayer fluids,[33,34] and its existence strongly argued against in a simulation study of idealized Brownian dipole lattices.[35] The last reference did however point out the impossibility of disentangling the contribution of the different shells, from a standard, time correlation function formalism standpoint. The energy flux formulation avoids such cross-correlation complications, and will be used to shed light on the ISE question for water by an investigation which necessitates a careful study of the long time scale solvent relaxation.

In the second half of this contribution, we will return to a special important aspect of the shorter time behavior, the water molecular axis rotational excitation. Here again, energy fluxes are particularly informative. In particular, we will see that these fluxes suggest that there is an intimate connection between the afore-mentioned asymmetry between energy channeled through rotations around each principal axis, and an initial asymmetry in the respective torques at the time of excitation. This connection will be supported and characterized in detail through the analysis of a substantial range of excitations.

The outline of the remainder of this paper is as follows. In the Section II, we briefly summarize the systems and parameters used in the simulations. The characterization of the water solvent spatial arrangements and analysis in terms of rotational and translational energy fluxes in different hydration shells of the electronically excited solute is addressed in Section III; the issue of the ISE is also examined here. Section IV explores—for the dominant short-time energy flow to water librations—the connection to the differing initial hydration shell structures for the solute whose charge will be changed in the excitation. Finally, we discuss the basic findings in Section V.

II. METHODS

In this contribution we will keep the same basic models as in I, with the limitation (as in II) that, given the negligible contribution of internal solvent vibrations reported in I, we consider only the (rigid) SPC/E model[36] for the solvent water molecules. For the solute, the model is taken (as in I and II) from Tran and Schwartz,[23] where the water-solute interaction consists of a Lennard-Jones interaction identical to the water-water LJ interaction, plus Coulomb interactions which depend on the solute charge. (We refer to I for comments on dipolar solutes and the present model's neglect of solute and solvent polarizability.[1]) All simulations have been run with an in-house code for one solute and 199 water molecules, with a cut-off distance of half the box length, and with the Ewald sum correction implemented for Coulomb forces. Equilibrium and nonequilibrium simulations have been run depending on the topic under discussion, and specific details will be provided when required. Most of the results correspond to nonequilibrium simulations, which consist of a long trajectory from which initial configurations are sampled. These configurations are used for independent separate nonequilibrium runs, where the solute charge is changed at $t = 0$, and along which the quantities of interest are calculated. Temperature control is maintained[37] during the generation of initial configurations, and turned off at the start of each non-equilibrium trajectory.

As in our previous contributions I and II, we separate the contribution of the different hydration layers. We recall that the first shell has been defined as enclosing all water molecules up to a maximum distance of 3.9 Å, a radius which on average contains roughly eight water

molecules (irrespective of the solute's charge), and for the second shell the distance chosen is 6.0 Å (see I for a detailed discussion of the rationale for these choices).

III. STRUCTURE AND ENERGY FLUXES

A. Structural changes after solute electronic excitation

We start by examining the substantial structural changes that take place after the electronically induced charge change in the solute. To guide this search, we display in Figure 2 the nonequilibrium solvation relaxation function $S(t)$, Eq. 1, i.e. the object amenable to experimental measurement, which is directly related to the solute time-dependent fluorescence emission frequency shift after the initial electronic excitation. As in I, we focus on a neutral monatomic solute that acquires a unit (positive or negative) charge, i.e. two systems with rather extreme changes in charge distribution. We recall that, for such systems, the normalized frequency shift function $S(t)$ can also be expressed as the normalized and shifted version of the total ion-water Coulomb energy $(V^c(t))$, i.e.

$$S(t) \equiv \frac{\overline{\delta\hbar\omega(t)} - \overline{\delta\hbar\omega(\infty)}}{\overline{\delta\hbar\omega(0)} - \overline{\delta\hbar\omega(\infty)}} = \frac{\overline{V^c(t)} - \overline{V^c(\infty)}}{\overline{V^c(0)} - \overline{V^c(\infty)}}, \quad (1)$$

where $\delta\hbar\omega$ corresponds to the instantaneous frequency shift from its vacuum value, and the overbars indicate a nonequilibrium average over trajectories. Finally, it is convenient to reorder terms and write $S(t)$ in terms of the newly-created ion-water Coulomb energy variation $(\Delta V^c(t) \equiv V^c(t) - V^c(0))$

$$S(t) = \frac{\overline{\Delta V^c(t)}}{\overline{V^c(0)} - \overline{V^c(\infty)}} + 1, \quad (2)$$

which provides a direct connection to the Coulomb interaction variation.

Figure 2 shows that the solvent relaxation is extremely fast: roughly 90% of the decrease has taken place in less than 0.5 ps, a time lapse during which marked oscillations can be observed, particularly for the positive ion. These oscillations display the same period in both cases, therefore signaling intrinsic features of the solvent dynamics. Indeed, they constitute the fingerprint of a common extremely efficient energy transfer into librational motion, as was first quantitatively shown in I, and to be discussed here in more detail. For the moment we just note that it is the high frequency water librations that are playing a significant role, as inferred from the oscillation period, which from Fig. 2 is ~ 0.04 ps, i.e. ~ 800 cm^{-1}.

In order to obtain a mechanistic understanding of how this fast energy transfer translates into structural changes within the water solvent, we first turn to inspection of standard functions that characterize positional and orientational order. Since these will now be time-dependent,
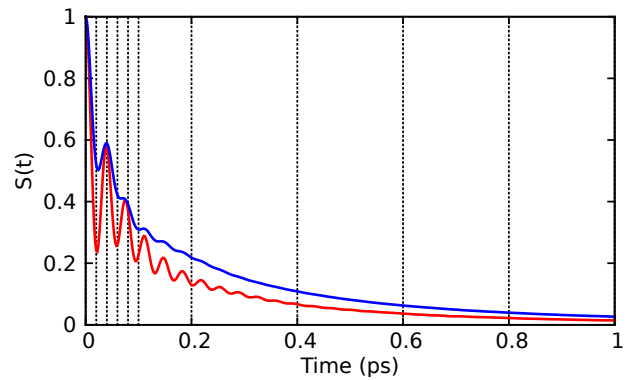

FIG. 2: Nonequilibrium frequency shift relaxation function $S(t)$, Eq. 1 for an aqueous solution containing a neutral solute acquiring upon electronic excitation at t=0 a positive (red curve) or negative (blue) unit charge. Structural properties are analyzed (see the text) at the times marked by vertical point lines: in view of the fast initial variation, six points have been taken in the 0-0.1 ps interval (i.e. a 0.02 ps interval, half of the period), after which the new intervals are taken to be one order of magnitude larger, i.e. 0.2 ps.

we select the times at which they will be computed being informed by the $S(t)$ behavior. The vertical lines in Fig. 2 denote the values chosen, although results will only be shown for a limited subset.

Figure 3 displays the results for the radial distribution function $g(r)$ characterizing the distribution of the monatomic solute-water center of mass distances. The main feature in connection with time scales is the remarkably slow onset of positional changes: even after $S(t)$ has already decreased to less than 30 % of its initial value (0.06 ps), there is hardly any signature of the first strong peak—located at ~ 2.9 Å for the cation, 2.6 Å for the anion— that will characterize the final equilibrium ionic hydration. A second aspect to note is that, as seen for example by comparing the curves for 0, 0.8 and 1 ps, the later stages are characterized by almost imperceptible changes, with which the system inches to its final equilibrium configuration. We will see in Sec. III B that these subtle changes play an unexpected central role in relation to the ISE issue.

The results for the solvent water molecular orientational changes are displayed in Fig. 4. As is standard, the orientational order has been characterized by the angle θ between the water center of mass-ion vector and the water dipole, sketched as an inset in Figure 4 (a). In contrast to the positional order, the water molecular orientation displays an extremely fast response to the newly created charge. It is remarkable that, starting from an almost flat distribution centered at 90°, and after just 0.02 ps (the first time analyzed, and coincident with half the period of high frequency librations), there has been a dramatic swing of θ for all the distances displayed. This is particularly true for the positive ion case in Fig. 4(a), for which the angle exceeds the final value in the 1 ps interval almost for every distance, while for the negative
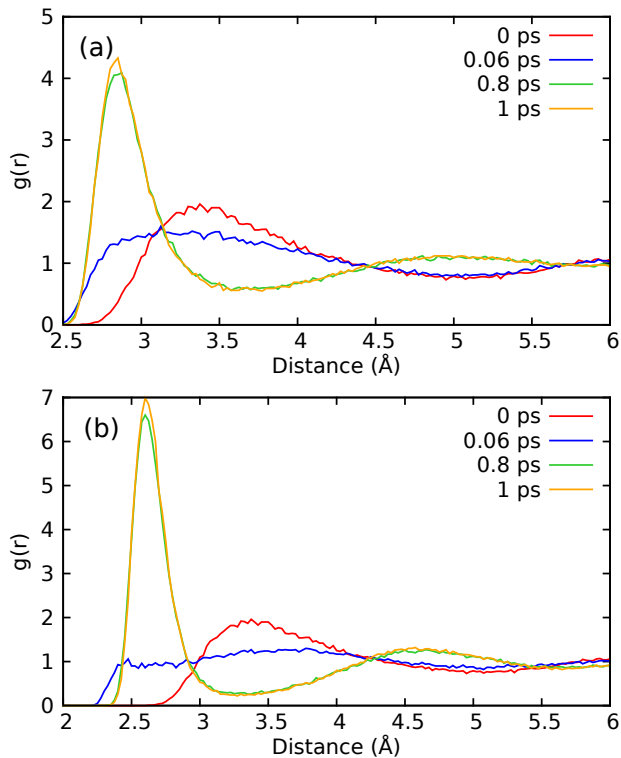
FIG. 3: Time evolution of the radial distribution function for the solute-water center of mass distance. (a) Solute excitation process $q = 0 \rightarrow q = +1$; (b) Process $q = 0 \rightarrow q = -1$

FIG. 4: Time evolution of the angle θ between water molecule dipole and oxygen-solute direction, see the sketch in the first panel. Solute excitation processes: (a) $q = 0 \rightarrow q = +1$; (b) $q = 0 \rightarrow q = -1$. Note that the shortest time displayed after excitation is 0.02 ps, to be compared with 0.06 ps in Fig. 3.

FIG. 5: Short time evolution of the angle θ between water molecule dipole and oxygen-solute direction, for the solute excitation process $q = 0 \rightarrow q = +1$.

ion this initial swing roughly equals the final equilibrium value if oscillations are averaged out. Actually, the main difference between the final equilibrium angle and that after only 20 fs is simply the lack of an oscillatory behavior for the latter: in effect, the subsequent time evolution just serves the purpose of reaching a more nuanced angle distribution, without changes comparable to the initial jump. It is interesting to note that the approach to equilibrium is underdamped, Fig. 5 displays, for the solute excitation process $q = 0 \rightarrow q = +1$, a more fine-grained short time evolution reaching only up to 0.08 ps, i.e. two full high frequency librational periods, with two samples per period. It can be seen that the curves oscillate back and forth during this time, and that the final oscillatory behaviour is not yet visible. This underdamped behavior in the orientational structural picture explains the high frequency ripples of $S(t)$, which as we have already stated are to be associated with librations.

B. Normalized energy fluxes

The previous subsection's discussion employed the conventional time-dependent versions of the equilibrium staples for configurational order analysis. We now go beyond these to the analysis of energy fluxes, first summarizing their relation to the solvation dynamics issue (I
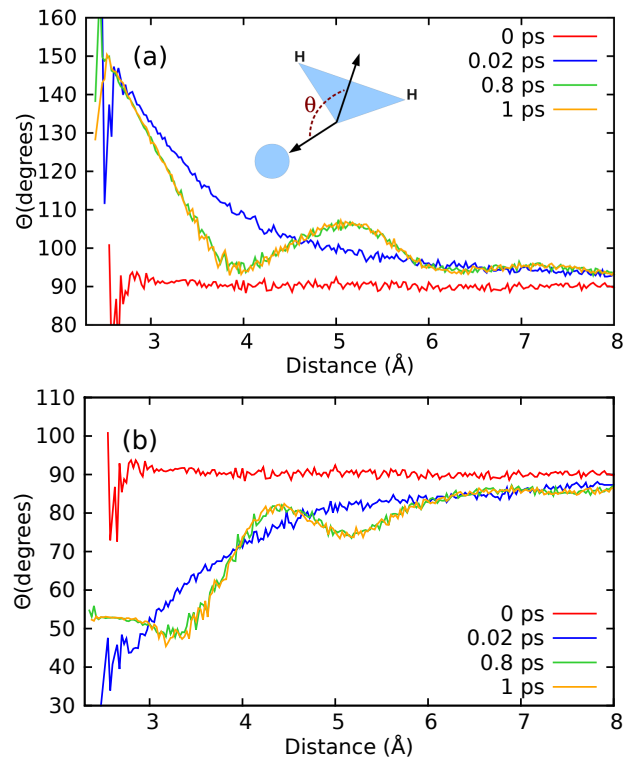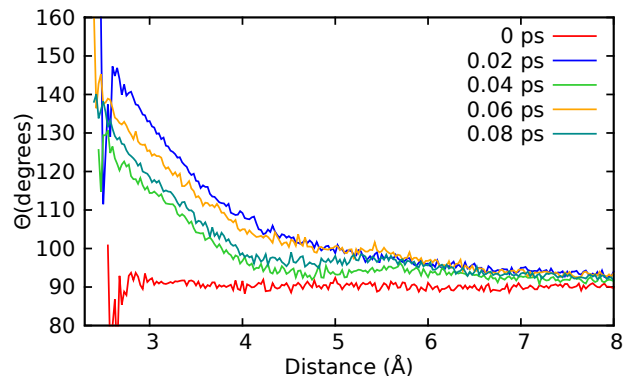
and II provide more complete accounts). For our initially neutral solute, rigid solvent systems, this consists of the simple formula for the nonequilibrium averaged variation of the Coulomb energy

$$\Delta V^c(t) = -W^T_{solute} - \sum_i W^T_i - \sum_i W^R_i. \qquad (3)$$

With Eq. 2, this equation directly connects the frequency shift functions to the work performed on the solute and

water solvent degrees of freedom. Here and in the following we suppress the overbar notation for notational ease. This energy variation simply transforms into work on solute translations (W_{solute}^{T}), solvent translations (W_i^{T}, with i denoting water molecules), and solvent hindered rotations (W_i^{R}). These contributions are easily computed during the simulation since they result from the time integrals of the force times the center of mass velocity for translational work, or the torque times angular velocity for rotations. These work contributions refer exclusively to ion-water Coulomb interaction, and do not include the rest of Coulomb interactions (nor non-Coulombic interactions).

Equation 3's crucial advantage is that it is clearly partitioned into molecular and mode contributions, i.e. we can unambiguously ascertain the participation of each molecule —or each hydration shell— and whether this contribution is related to the molecule's translation and/or libration, without any complication from cross terms. As we demonstrated in I, the picture conveyed by this approach is remarkably clear. For example, for the case of a newly created solute positive charge, Fig. 6 displays the results for the work on the rotations and translations.
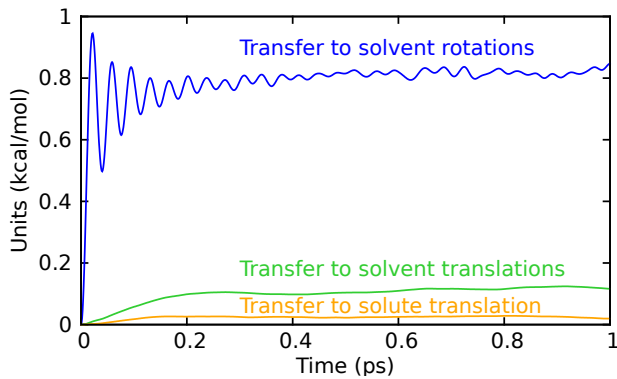

FIG. 6: Contributions of the nonequilibrium work on different molecular motions resulting from the solute charge creation process $q = 0 \rightarrow q = +0.1$ in water solvent (in units of electron charge).

The figure shows that after short lived initial transients, equilibrium is characterized by the several plateaus indicating that 78.6 % of the total energy transferred is channeled to librations of the water molecules neighboring the solute, with a much less important transfer into translations of the solvent waters (18.6 %), and only 2.8 % taken up by the now ionic solute's translational motion. Similar results are found for a created negative ion (not shown): librations 72 %, translations 21.5 %, and 6.5 % to ion translations. The picture of the overwhelming role of transfer into librations is very robust, with only minor variations (other charge changes have been explored with similar results, see II).

We have determined that the hydration shell-dependent information on the flux results can be very

usefully presented in a form which emphasizes time scales. In particular, we will compare the preceding time-dependent work contributions after they are normalized by fixing a unit value for their respective plateaus. This makes evident whether there exists a definite difference of time scales for the various contributions to the work exerted on each hydration shell. Somewhat surprisingly (at least initially), such an analysis requires simulation runs substantially longer than e.g. that shown in Fig. 6, which seems to show that equilibrium has been attained in ~ 1 ps. But in retrospect, this requirement for the establishment of equilibrium for more restricted spatial regions in Figs. 3 and 4 is consistent with the long times that can be associated with the full completion of structural equilibrium in water.[38,39] Thus, our nonequilibrium trajectories will be taken to be 10 ps long, with a time step of 2 fs, and the associated results will be averaged over 20 independent runs, each including 5000 trajectories. Finally, all work functions will be normalized to their average value for the last 0.5 ps, i.e. within the interval [9.5,10] ps.
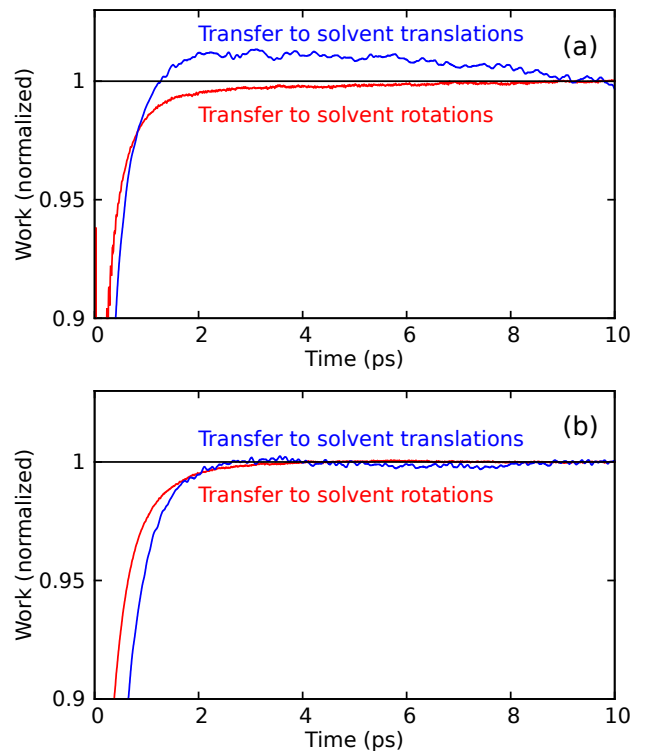

FIG. 7: Normalized contributions to the work on the water solvent librations and translations (note the reduced range on vertical axis). Solute excitations: (a) $q = 0 \rightarrow q = +1$; (b) $q = 0 \rightarrow q = -1$.

Figure 7 displays the total normalized contributions to the work on rotation and translation of the water solvent for both excitation-induced solute charge change cases. It can be seen that the time scale for energy transfer into translation is longer than that for transfer into librations. This is particularly evident for the created positive ion,

with a non-monotonic behavior for translations. The produced anionic solute case exhibits a smaller difference, although a delay between the two transfers is still clearly visible for times shorter than 1 ps. But a much richer picture emerges if the total contributions of the work on translations and rotations are decomposed into their contributions from different hydration shells. The results for the positive ion case are displayed in Fig. 8, with both panels having the same vertical range, so that the time scales can be directly compared.
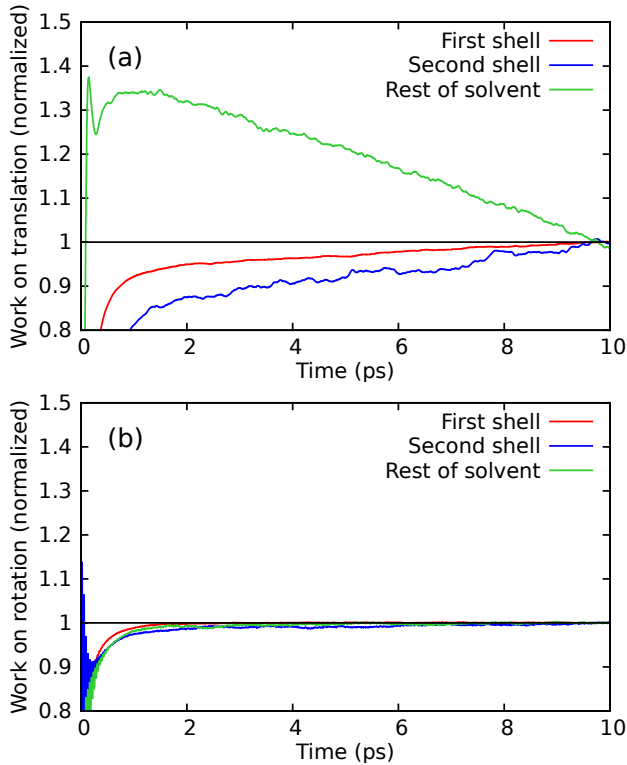

FIG. 8: The normalized work contributions for different hydration shells for the solute excitation process $q = 0 \to q = +1$: (a) Work on water solvent translations; (b) Work on water solvent hindered rotations. The hydration shells are defined in the Methods Section.

The most remarkable aspect revealed in Fig. 8—and a main result of the present contribution—is that the translational work time scales (panel (a)) show a well defined dependence on hydration shell: the work on the first shell molecules (red curve) has the faster decay towards its normalized value at 10 ps, followed by the work on the second shell molecules (blue curve) and, finally, the most slowly decaying work on the rest of the solvent. We pause to remark that this plot also illustrates why long trajectories are required to uncover these features: even our 10 ps long trajectories are not sufficient to reach full equilibrium, as saturation has not been fully reached, but our goals neither include nor require the absolute time scales for the full equilibration. Turning to the water librations in panel (b), a message similar to that for translation is conveyed but it is considerably muted. The least ambigu-
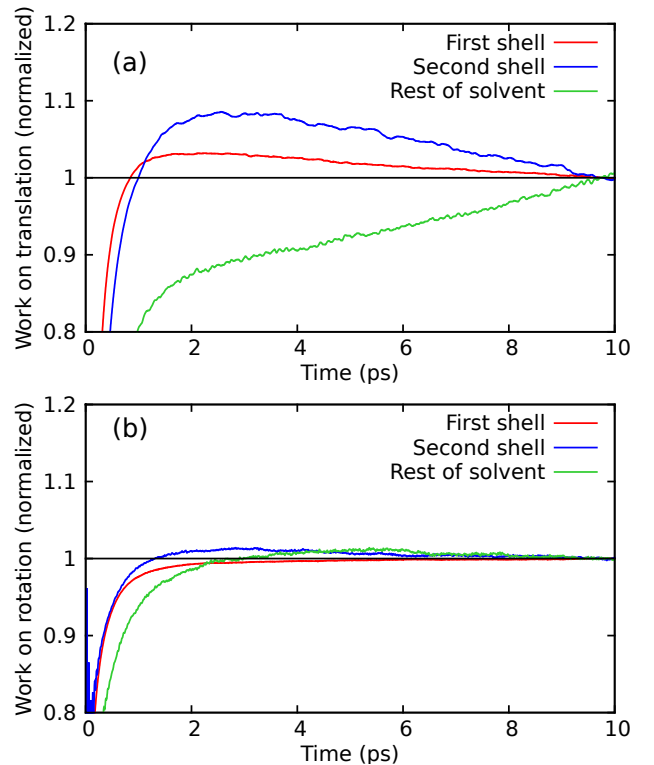

FIG. 9: The normalized work contributions for the different hydration shells for the solute excitation process $q = 0 \to q = -1$: (a) Work on water solvent translations; (b) Work on water solvent hindered rotations. The hydration shells are defined in the Methods Section.

ous aspect might be that the work on the water molecules beyond the second shell has a slightly longer time scale.

Figure 9 shows that these basic patterns also hold for a solute excitation producing an anion. We again see a clear trend for the work on translations, with the energy transfer to the outer water molecules being the slowest, and again slightly slower energy transfer into water librations in the outer shells. All the differences for the anionic solute case are less marked than for the positive ion solute case, as indicated by the fact that the Fig. 9 vertical scale has a smaller interval compared to that of Fig. 8. These smaller differences were to be expected from the behavior displayed in Fig. 7.

To summarize, our energy flux results—which do not suffer from the cross terms that complicate time correlation function analyses—clearly indicate that, in response to charge changing excitations for a solute in water, a difference in time scales between the different hydration shells indeed exists. This effect is essentially confined to the water translations, which is the minority channel for aqueous solvation energy relaxation —and to a much lesser extent to the water librations, whose work contributions display a much less dramatic distance dependence, with a first hydration shell relaxation rate slightly faster than the second and remaining hydration shells. The direction of the differential hydration shell behav-

ior for translation—longer time scales for outer shells—could be termed a snowball effect, rather than the extensively discussed inverse snowball effect. Finally, since most of the excess energy is channeled through rotations, the present problem does not seem to conform with the theoretical prediction[29] of a snowball effect being associated to processes dominated by excess energy transfer to translations.

IV. ROTATIONAL WORK AND INITIAL TORQUE

A. Principal axes asymmetry

The last portion of Sec.III fastened on the long time behavior for the water solvent response, which we found to be controlled by translations in a subtle fashion. But as shown e.g. in Fig. 6, the short time energy flow into water librations overwhelmingly plays the dominant role in the solvent relaxation.

Here we address an intriguing feature of that dominant energy flow which is in fact determined by structural effects, the basic theme of this work. The energy flow analyses in I and II revealed that when the solute electronic excitation-induced work on the water librations was partitioned among principal axes of the solvent water molecules, most of the energy was found to be channeled through hindered rotations around the axis (through the center of mass) parallel to the H-H axis between the hydrogens of the molecule; this is the x axis in Fig. 10 (see the inset for axes definition). An illustrative example is displayed in that same Figure, corresponding to the very small solute negative charge creation process $q = 0 \rightarrow -0.1$. Similar plots can be found in I, corresponding to a final charge one order of magnitude larger, i.e. $q = 0 \rightarrow -1$ (see Fig. 10(a) in I), or with opposite sign ($q = 0 \rightarrow 1$, Fig. 9(a) in I). These observations uncover two related and unexpected features: a remarkable asymmetry between principal axes (with a dominance of the x axis), and a surprising independence of this effect on the charge magnitude and sign of the newly created solute charge.

Since the solvent's hydration structures differ dramatically for anions and cations, with a water's dipole moment typically pointing in roughly opposite directions (see Fig. 1 for a qualitative view, and Fig. 4 for a more quantitative perspective), one would expect that any asymmetry should depend on the solute's charge sign and be heavily influenced by its absolute value as well. It is thus puzzling that none of these factors seems to play a significant role. An explanation along the lines that energy transfer should be faster into axes characterized by a lower moment of inertia has already been discarded in I, since there is no well-defined order: most of the work is channeled through the x axis (smallest moment of inertia), followed by the z axis (largest), and with a minor transfer into rotations around the y axis (intermediate).
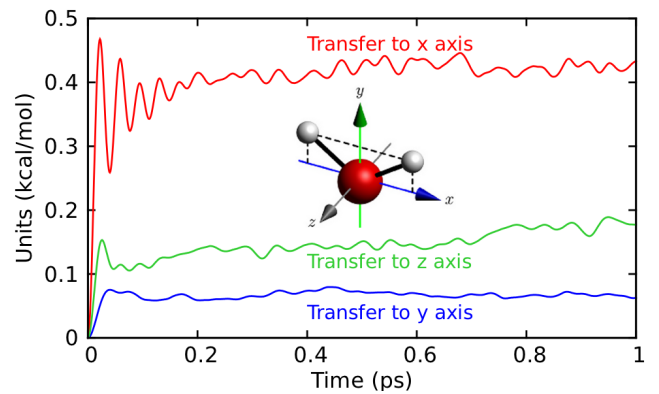

FIG. 10: Transfer into the water molecule rotational body-fixed axis, of the first hydration shell water molecules, for the solute electronic transition $q = 0 \rightarrow q = -0.1$ and rigid water solvent model. See the text and sketch in the inset for the definition of axes, and the Computational Details section for the definition of shells.

Before proceeding, it should be kept in mind that in all the examples discussed the water solvent starts from an equilibrium configuration characterized by an uncharged solute, and the puzzle might be specific to this particular case. The initially neutral case has been the workhorse for most ionic solvation relaxation studies. Of course, this choice is a reasonable one for a monatomic solute, since it corresponds to the loss or acquisition of an electron. Nevertheless, we will explore other (fractional) charge changes to assist in the resolution of our puzzle. This is of some interest in connection with molecular solutes, where electronic excitations can be modeled in terms of accompanying changes of (fractional) site charges.

B. Torque-energy flux connection

The basic observation that will guide our analysis is that the asymmetry—in which the energy flow is through water librations around the water molecular x axis parallel to the water's H-H axis (cf Fig.10 insert)—is evident from very short times, and extends monotonically to longer times, i.e. without crossings among the curves corresponding to the work on each of the axes; Figure 10 furnishes a fair illustration of the generic behavior found in all the cases analyzed. These features suggest an important potential connection with structure: that the final outcome reflecting these features may be to a significant extent due to a structural asymmetry in the solvent present from the very beginning, i.e. before the charge-changing excitation. And since the work on a water molecule's hindered rotation results from the scalar product of torque times angular velocity, the relevant driving "initial plus" (IP) torque might be directly related to this driving factor. By IP torque we mean the torque on the water solvent molecules produced at time $t = 0+$ by the charge generated by the excitation

in the solute but with those solvent molecules still in their spatial configurations existing before the excitation at time $t = 0$. In brief, this is the torque arising from the immediately post-excitation solute charge interacting with the water molecules in their pre-excitation configurations. For example, the IP torque is that experienced by the water solvent molecules in their $t = 0$, uncharged $q = 0$ solute, equilibrium distribution of configurations—for which there is obviously no Coulombic torque—but now subject to the instantaneously newly created at $t = 0+$ finite solute charge. There can now be an average torque in the presence of this charge. But note that the IP categorization refers to a time $t = 0+$ such that the water molecules have no time to react to the torque now experienced. For cases where the solute has a finite charge before the excitation, there will be individual torques on the waters (exerted by the ion); now the IP torque would refer to the total torque (again, exerted by the ion) on the water molecules which were still in their pre-existing configuration determined by the new excitation charge in the solute. Indeed, such a relation would immediately explain that results quoted at the beginning of this Section are largely independent of sign: once an ion is created, the absolute value of the torque's projection on each principal axis will be already determined by the solvent's molecule's pre-existing equilibrium distribution set by the vanishing pre-excitation charge, and thus be independent of a change of the newly created ion's charge sign. A similar reasoning would account for the non-dependence on the produced ionic charge's absolute value in the cases described above: in general, a modest increase would just produce a larger modulus for the torque, but would not change the relative proportions among the torques for the water molecule's three principal axes, since the water molecule's distribution was previously established by the pre-existing zero charge.

We thus proceed to ascertain if indeed there is a correlation between the IP torque on a given principal axis and the final rotational work channeled through it. All of the previous examples correspond to a process characterized by a solute charge change of the type $q = 0 \rightarrow q'$. We now want to probe into a larger set, also allowing for a pre-excitation charge q different from zero, i.e. $q \rightarrow q'$. The corresponding parameter space to explore is not as large as one might initially estimate. In the simple case of a monatomic solute, and as previously noted, the torque the ion exerts on a given molecule is obviously proportional to the ion's charge. Therefore, since we are only interested in, and will calculate, the *relative* weight of the IP torque's projection on each principal axis, the actual value of q' is irrelevant. We thus only need to concern ourselves with selecting a certain range for the pre-excitation charge q determining the solvent's initial equilibrium distribution (we take $q \in [-1, 1]$), and compute the IP torque for an arbitrary newly created charge (q'); this IP torque is calculated before the water molecules can react to the IP torque. To be more specific, for a given value of q a long equilibrium simula-

tion is run during which, at sufficiently separated times, we compute the torque exerted on its neighbors if this charge would be instantaneously switched to q' (a different, positive or negative charge). Again this computation is effected before the water molecules can react to the IP torque. As indicated above, we are concerned with the IP torque magnitudes. The normalized projections of this IP torque on each molecule of the solute's first hydration shell —defined as its closest eight water molecules— are subsequently averaged, which results in the following convenient set of three indexes

$$\left(\left\langle \frac{\tau_x^2}{\|\tau\|^2} \right\rangle, \left\langle \frac{\tau_y^2}{\|\tau\|^2} \right\rangle, \left\langle \frac{\tau_z^2}{\|\tau\|^2} \right\rangle \right), \qquad (4)$$

where τ_α denotes the projection of the molecular torque on principal axis α.

Figure 11 displays the results obtained for all three indexes as a function of initial, pre-excitation charge. The first aspect to notice is that indeed a clear-cut order exists for all cases, i.e. the average values for each component are not identical for any value of the solute's initial charge q. We first consider the case $q = 0$ for the pre-excitation charge, which corresponds to almost all the instances discussed in I and II. We observe that the ordering of axes is indeed identical with that found in Fig. 10 for the final channeled work contributions (even though here the final charge is +1 and in Fig. 10 it is -0.1). While at this point it is not possible to discard other factors, this strongly suggests that an extremely important factor determining the role of each principal water rotational axis comes from the value of the corresponding (new charge-induced) torque governed by the pre-excitation equilibrium water molecule distribution.

The next point of interest is that Figure 11 also takes a first step in addressing whether this strong correlation just discussed between the initial induced torque and energy channeled through each principal axis extends beyond the initially neutral solute to a larger set of pre-excitation solute charges. It is seen in Fig. 11 that the x and z axis switch their roles in the neighborhood of $q \sim -0.5$, with the y axis playing a secondary role in all cases. The x-axis dominance—and indeed the ordering of axes—for charges to the right of this threshold is the same that as that found for energy transfer in the neutral to charged solute examples discussed in I and II, and in Fig. 10. But our calculations have now revealed that in some cases ($q \leq -0.5$) the dominant torque is found for the z axis. Therefore an exacting test of the torque/channeled energy correlation can be made by checking whether a crossing between x and z axes is also found for the total energy channeled through each principal axis. This is now undertaken.

For our test, we will present the results of two different sets of charge excitation results. In the first set, we have focused on a subset of charge changes (averaging over sets of 500 trajectories), in which computations have
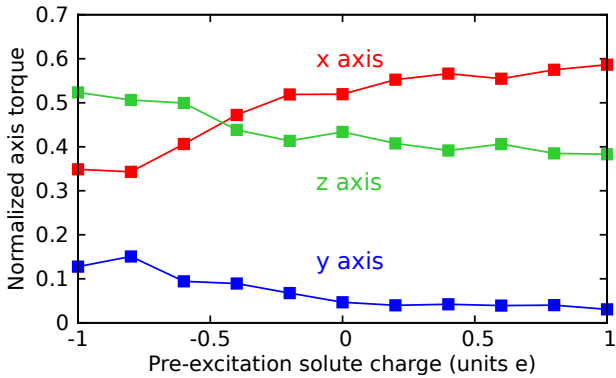
FIG. 11: Normalized average initial induced torque on the principal axes of first shell hydration molecules (see Eq. 4—and its surrounding text—for the quantitative definition and Fig. 10 for the definition of the system axes). The abscissa represents the different initial pre-excitation charges defining the initial equilibrium configurations of the solvent molecules. In each computed case, there is then a change in the charge to produce a fixed final charge: the torque is computed such that the excited solute's charge change produces the excited charge $+1$ (for the case $q = 1$, a small charge -0.1 is used since the existing charge is already $+1$). The squares correspond to the cases computed, with lines providing a guide to the eye.
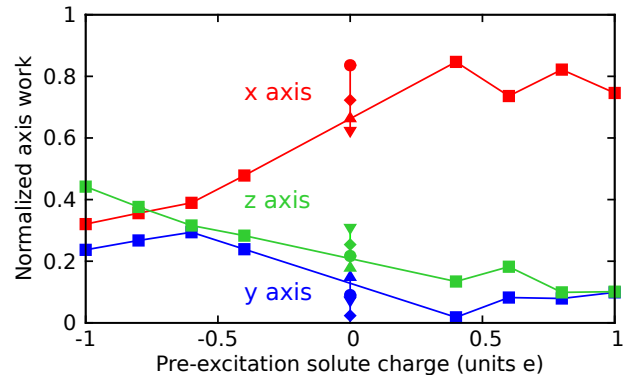

FIG. 12: Total final hindered rotational work channeled through each of the three water molecule rotational principal axes for the first shell molecules, as extracted from the corresponding plateaus (see different plateau values for instance in Fig. 10, which also defines the water axis system). The squares correspond to the processes $q \to \pm 0.2$, with the sign depending on, and the same as, the sign of pre-excitation solute charge q (see the text). Also included are the vertically arranged symbols for the fixed initial charge situation $q = 0$, corresponding to the excitation processes with different final solute charges q': $q = 0 \to q'$ (diamond: $q' = +1$; circle: $q' = +0.2$; triangle: $q' = -0.2$; inverted triangle: $q' = -1$).

been performed of the set $q \to -0.2$ (for negative pre-excitation solute charges $q = 0, -0.4, -0.6, -0.8, -1$), and $q \to +0.2$ (for positive pre-excitation solute charges $q = 0, 0.4, 0.6, 0.8, 1$). These results for the final work contributions scan the same range of pre-excitation charges as does Fig. 11, but all have different final charges than in that Figure. Results for the final work contributions channeled through each principal axis, expressed as the percentage of the total work channeled into rotations of the first shell, are summarized in Fig. 12.

Although it is obvious that details of the induced torque results in Fig. 11 are not reproduced quantitatively in Fig.12, the patterns in both plots are qualitatively similar. The water y rotational axis contribution is in all cases a minority contribution, and a crossover from a dominance of the x axis to that of the z axis does occur, albeit for charges slightly lower that the Fig. 11 location at ~ -0.5.

Our second test of *final* work contributions results in Fig. 12 is focused on the following issue. In contrast to the situation for the short time torque for the processes $q \to q'$ with a generally finite pre-excitation solute charge q, there is no *a priori* reason to expect the final work for each water molecule rotational axis to be independent of the final charge q'; although the latter is created rapidly, the final work requires time to be established, as already illustrated in e.g. Fig. 8. We especially illustrate this point for the important case of an initial neutral solute ($q = 0$) by including the final work results for the processes $q = 0 \to \pm 0.2, \pm 1$, which in Fig. 12 are linked by vertical lines at $q = 0$ (note that the final charge q' is

now covering the interval $[-1, 1]$). While there is clearly a non-negligible dispersion for each axis, the qualitative behavior of the final rotational work plateau values is robust with respect to these substantial variations. In short, the curves displayed in Fig. 12 while just a sample representing broader distributions, are seen to effectively be correlated to a considerable extent with the initial induced torque.

V. CONCLUDING REMARKS

We start by emphasizing the capabilities of the tool used here, i.e. the computation of nonequilibrium energy fluxes illustrated in the present context after a sudden solute charge change and the subsequent water solvent response. This tool facilitates a detailed analysis of the different contributions, both in terms of spatial distribution (hydration shells) and modes of motion (librations (hindered rotations)/translations, molecular principal rotation axes, etc.). This approach opens a new window on the subject of "solvation dynamics", as it provides for the first time highly detailed quantitative molecular level information, which among its attractive attributes numbers the lack of the obscuring complexity and ambiguity associated with the cross correlations present in time correlation function calculations. As such, it seems potentially as promising as in its application to vibrational[12,13] and rotational relaxation.[14]

In the present effort, the computation of the time-dependent energy fluxes for water molecule hindered rotations and translation—together with the calculation of

positional and orientational distributions— has easily uncovered the range of time scales involved in structural, i.e. orientational and positional, relaxation after an electronic charge-changing excitation of the solute. On the short time scales dominated by librational energy flow, the orientational order of the water solvent is roughly achieved in just half a librational period. For the longer time scale solvation dynamics, we have presented evidence supporting the notion of a fast librational relaxation operating over at least nanometer length scales (our approximate box size), which is fastest in the first hydration layer, accompanied by a slower and much more pronounced water molecule positional reordering which proceeds from a newly created ion outwards; this subtle "snowball" effect—which is the opposite of the often-discussed "inverted snowball" effect—has previously remained elusive.

We have also addressed the prevalence of energy transfer into the rotational axis parallel to the water molecule's H-H direction, a finding reported in I, a previously unnoticed feature uncovered via energy flux computations. Calculations and arguments have been presented indicating that this phenomenon reflects an structural asymmetry of immediate post-excitation torques on water molecules surrounding a monatomic solute. This structural effect is shown to be an important factor that conditions the rotational work through each principal axis, the work we have shown is the dominant water solvent relaxation channel in the solvent dynamics. These features emphasize the relation between the water solvent structure and energy flows, a central theme of this work.

* Electronic address: rosendo.rey@upc.edu
† Electronic address: hynes@spot.colorado.edu

BIBLIOGRAPHY

[1] Rey, R.; Hynes, J.T. Solvation Dynamics in Liquid Water. I. Ultrafast Energy Fluxes. *J. Phys. Chem. B*, **2015**, *119*, 7558-7570.

[2] Rey, R.; Hynes, J.T. Solvation Dynamics in Liquid Water. II. Energy Fluxes on Ground and Excited State Surfaces. *J. Phys. Chem. B* **2016**, *120*, 11287-11297.

[3] Bagchi, B. Dynamics of Solvation and Charge-Transfer Dynamics in Liquids. *Ann. Rev. Phys. Chem.* **1989**, *40*, 115-141.

[4] Maroncelli, M.; Macinnis, J.; Fleming, G.R. Polar-Solvent Dynamics and Electron-Transfer Reactions. *Science* **1989**, *243*, 1674-1681.

[5] Fleming, G.R.; Wolynes, P.G. Chemical Dynamics in Solution. *Phys. Today* **1990**, *43*, 36-43.

[6] Fleming, G.R.; Cho, M.H. Chromophore-Solvent Dynamics. *Ann. Rev. Phys. Chem.* **47**, *47*, 109-134.

[7] Cho, M.; Fleming, G.R. Electron Transfer and Solvent Dynamics in Two- and Three-State Systems. *Adv. Chem. Phys.* **1999**, *107*, 311-370.

[8] Nandi, N.; Bhattacharyya, K.; Bagchi, B. Dielectric Relaxation and Solvation Dynamics of Water in Complex Chemical and Biological Systems. *Chem. Rev.* **2000**, *100*, 2013-2045.

[9] Maroncelli, M. The Dynamics of Solvation in Polar Liquids. *J. Mol. Liq.* **1993**, *57*, 1-37.

[10] Stratt, R.M.; Maroncelli, M. Nonreactive Dynamics in Solution: The Emerging View of Solvation Dynamics and Vibrational Relaxation. *J. Phys. Chem.* **1996**, *100*, 12981-12996.

[11] Bagchi, B.; Jana, B. Solvation Dynamics in Dipolar Liquids. *Chem. Soc. Rev.* **2010**, *39*, 1936-1954.

[12] Rey, R.; Ingrosso, F.; Elsaesser, T.; Hynes, J.T. Pathways for H_2O Bend Vibrational Relaxation in Liquid Water. *J. Phys. Chem. A* **2009**, *113*, 8949-8962.

[13] Rey, R.; Hynes, J.T. Tracking Energy Transfer from Excited to Accepting Modes: Application to Water Bend Vibrational Relaxation. *Phys. Chem. Chem. Phys.* **2012**, *14*, 6332-6342.

[14] Petersen, J.; Møller, K.B.; Rey, R.; Hynes, J.T. Ultrafast Librational Relaxation of H_2O in Liquid Water. *J. Phys. Chem. B* **2013**, *117*, 4541-4552.

[15] Maroncelli, M.; Fleming, G.R. Computer Simulation of the Dynamics of Aqueous Solvation. *J. Chem. Phys.* **1988**, *89*, 5044-5068.

[16] Perera, L.; Berkowitz, M.L. Dynamics of Ion Solvation in a Stockmayer Fluid. *J. Chem. Phys.* **1992**, *96*, 3092-3101.

[17] Roy, S.; Bagchi, B. Solvation Dynamics in Liquid Water. A Novel Interplay between Librational and Diffusive Modes. *J. Chem. Phys.* **1993**, *99*, 9938-9943.

[18] Nandi, N.; Roy, S.; Bagchi, B. Ionic and Dipolar Solvation Dynamics in Liquid Water. *Proc. Indian Acad. Sci. (Chem. Sci.)* **1994**, *106*, 1297-1306.

[19] Nandi, N.; Roy, S.; Bagchi, B. Ultrafast Solvation Dynamics in Water: Isotope Effects and Comparison with Experimental Results. *J. Chem. Phys.* **1995**, *102*, 1390-1397.

[20] Re, M.; Laria, D. Dynamics of Solvation in Supercritical Water. *J. Phys. Chem. B* **1997**, *101*, 10494-10505.

[21] Koneshan, S.; Rasaiah, J.C.; Lynden-Bell, R.M.; Lee, S.H. Solvent Structure, Dynamics, and Ion Mobility in Aqueous Solutions at 25 C. *J. Phys. Chem. B* **1998**, *102*, 4193-4204.

[22] Biswas, R.; Bagchi, B., Ion Solvation Dynamics in Supercritical Water. *Chem. Phys. Lett.* **1998**, *290*, 223-228.

[23] Tran, V.; Schwartz, B.J. Role of Nonpolar Forces in Aqueous Solvation: Computer Simulation Study of Solvation Dynamics in Water Following Changes in Solute Size, Shape and Charge. *J. Phys. Chem. B* **1999**, *103*, 5570-5580.

[24] Aherne, D.; Tran, V.; Schwartz, B.J. Nonlinear, Nonpolar Solvation Dynamics in Water: the Roles of Electrostiction

and Solvent Translation in the Breakdown of Linear Response. *J. Phys. Chem. B* **2000**, *104*, 5382-5394.

[25] Rasaiah, J.C.; Lynden-Bell, R.M. Computer Simulation Studies of the Structure and Dynamics of Ions and Non-Polar Solutes in Water. *Phil. Trans. R. Soc. Lond. A* **2001**, *359*, 1545-1574.

[26] Duan, J.; Shim, Y.; Kim, H.J. Solvation in Supercritical Water. *J. Chem. Phys.* **2006**, *124*, 204504.

[27] Maroncelli, M.; Fleming, G.T. Picosecond Solvation Dynamics of Coumarin 153: the Importance of Molecular Aspects of Solvation. *J. Chem. Phys.* **1987**, *86*, 6221-6239.

[28] Karim, O.A.; Haymet, A.D.J.; Banet, K.J.; Simon, J.D. Molecular Aspects of Nonequillbrium Solvation: A Simulation of Dipole Relaxation. *J. Phys. Chem* **1988**, *92*, 3391-3394.

[29] Chandra, A.; Bagchi, B. Breakdown of Onsager's Conjecture on Distance Dependent Polarization Relaxation in Solvation Dynamics. *J. Chem. Phys.* **1989**, *91*, 2594-2598.

[30] Tachiya, M. An Alternative Interpretation of Onsager's Inverted Snowball Effect of Electron Solvation. *Chem. Phys. Lett.* **1993**, *203*, 164-165.

[31] Bedard-Hearn, M.J.; Larsen, R.E.; Schwartz, B.J. Understanding Nonequilibrium Solute and Solvent Motions through Molecular Projections: Computer Simulations of Solvation Dynamics in Liquid Tetrahydrofuran (THF). *J. Phys. Chem. B* **2003**, *107*, 14464-14475

[32] Maroncelli, M. Computer Simulations of Solvation Dynamics in Acetonitrile. *J. Chem. Phys.* **1991**, *94*, 2084-2103.

[33] Perera, L.; Berkowitz, M.L. Dynamics of Ion Solvation in a Stockmayer Fluid. *J. Chem. Phys.* **1992**, *96*, 3092-3101.

[34] Neria, E.; Nitzan, A. Simulations of Solvation Dynamics in Simple Polar Solvents. *J. Chem. Phys.* **1992**, *96*, 5433-5440.

[35] Papazyan, A.; Maroncelli, M. On the Validity of the "Inverted Snowball" Picture of Solvation Dynamics. *J. Chem. Phys.* **1993**, *98*, 6431-6436.

[36] Berendsen, H. J. C.; Grigera, J.R.; Straatsma, T.P. The Missing Term in Effective Pair Potentials. *J. Phys. Chem* **1987**, *91*, 6269-6271.

[37] Berendsen, H.J.C.; Postma, J.P.M.; van Gunsteren, W.F.; DiNola, A.; Haak, J.R. Molecular Dynamics with Coupling to an External Bath. *J. Chem. Phys.* **1984**, *81*, 3684-3690.

[38] Sciortino, F.; Sastry, S. Sound Propagation in Liquid Water: The Puzzle Continues. *J. Chem. Phys.* **1994**, *100* 3881-3893.

[39] Berne, B.J.; Pecora, R. *Dynamic Light Scattering*; Courier Dover Publications: New York, USA, 2000.

TABLE OF CONTENTS IMAGE